BEST AVAILABLE IMAGES

Defective images within this document are accurate representations of the original documents submitted by the applicant.

Defects in the images may include (but are not limited to):

- BLACK BORDERS
- TEXT CUT OFF AT TOP, BOTTOM OR SIDES
- FADED TEXT
- ILLEGIBLE TEXT
- SKEWED/SLANTED IMAGES
- COLORED PHOTOS
- BLACK OR VERY BLACK AND WHITE DARK PHOTOS
- GRAY SCALE DOCUMENTS

IMAGES ARE BEST AVAILABLE COPY.

As rescanning documents *will not* correct images, please do not report the images to the Image Problem Mailbox.

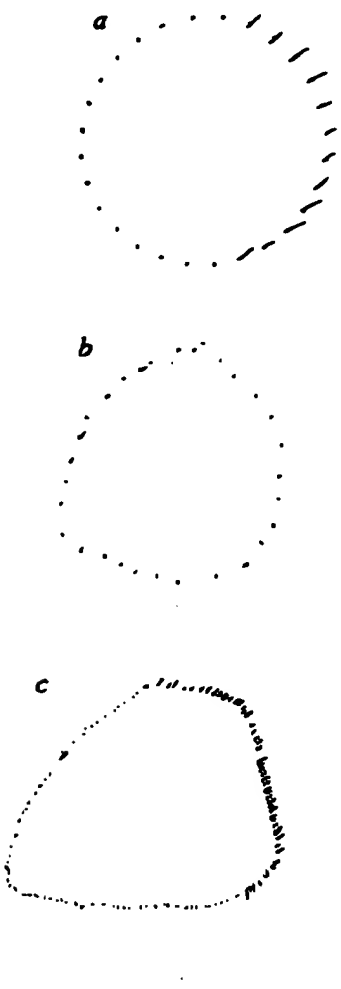

FIG. 4 J.R.'s attempts to cancel the local components of a predrawn figure (*a*); to reproduce the figure (*b*); and to draw the figure and then cancel its local components (*c*).

even when focal attention cannot be automatically directed to local components on the left of a global figure. J.R.'s neglect is thus neither purely perceptual nor purely motor; it rather arises from an input-deficit to a 'premotor' mechanism[10] committed to the exogenous control of focal attention. Lesions that 'disrupt the cross-talk between inferior posterior areas' can reduce or eliminate interactions between global and local processing[9]. Whether this disruption in J.R. is due solely to her right hemisphere lesion (or also implicates her left thalamic infarct) is unclear. One further problem remains: why is J.R. unaware of the discrepancy between her global percepts and local actions? The process of local completion can mask perceptual incongruity but cannot then control appropriate manual output. J.R. can perceive the whole forest but cannot use that percept to search for and cut down the trees on the left thereof. □

Received 6 September; accepted 12 December 1994.

1. Marshall, J. C. & Halligan, P. W. *Nature* **336**, 766–787 (1988).
2. Halligan, P. W. & Marshall, J. C. *Cogn. Neuropsychol.* **11**, 187–206 (1994).
3. Navon, D. *Cogn. Psychol.* **9**, 353–383 (1977).
4. Sergent, J. *Brain* **111**, 347–373 (1988).
5. Bottini, G., Sterzi, R. & Vallar, G. *J Neurol. Neurosurg. Psychiat.* **55**, 562–565 (1992).
6. Halligan, P. W. & Marshall, J. C. *Cortex* **30**, 685–694 (1994).
7. Kinsbourne, M. *Trans. Am. Neurol. Assoc.* **95**, 143–145 (1970).
8. Ladavas, E., Del Pesce, M., Mangun, G. R. & Gazzaniga, M. S. *Cogn. Neuropsychol.* **11**, 57–74 (1994).
9. Robertson, L. C. in *Cognitive Neuropsychology in Clinical Practice* (ed. Mangolin, D. I.) 70–95 (Oxford University Press, New York, 1992).
10. Rizzolatti, G. & Berti, A. *Rev. Neurol.* **146**, 626–634 (1990).

ACKNOWLEDGEMENTS. This work was supported by the Medical Research Council.

Alzheimer-type neuropathology in transgenic mice overexpressing V717F β-amyloid precursor protein

Dora Games*, David Adams†‡, Ree Alessandrini†, Robin Barbour*, Patricia Berthelette†‡, Catherine Blackwell†‡, Tony Carr*, James Clemens§, Thomas Donaldson†‡, Frances Gillespie†‡, Terry Guido*, Stephanie Hagopian†‡, Kelly Johnson-Wood*, Karen Khan*, Mike Lee*, Paul Leibowitz†‡, Ivan Lieberburg*¶, Sheila Little§, Eliezer Masliah‖, Lisa McConlogue*, Martin Montoya-Zavala†‡, Lennart Mucke☆, Lisa Paganini*, Elizabeth Penniman†, Mike Power*, Dale Schenk*, Peter Seubert*, Ben Snyder†, Perdie Soriano*, Hua Tan*, James Vitale†‡, Sam Wadsworth†‡, Ben Wolozin & Jun Zhao***

* Athena Neurosciences, Inc., 800 Gateway Boulevard, South San Francisco, California 94080, USA
† Exemplar Corporation, One Innovation Drive, Worcester, Massachusetts 01605, USA
§ Lilly Research Laboratories, Indianapolis, Indiana 46285, USA
☆ The Scripps Research Institute, Department of Neuropharmacology, 10666 North Torrey Pines Road, La Jolla, California 92037, USA
‖ Department of Neurosciences, University of California, San Diego, 9500 Gilman Drive, La Jolla, California 92093, USA
** Laboratory of Clinical Science, National Institute of Mental Health, 9000 Rockville Pike, 10D41, Bethesda, Maryland 20892, USA

ALZHEIMER'S disease (AD) is the most common cause of progressive intellectual failure in aged humans. AD brains contain numerous amyloid plaques surrounded by dystrophic neurites, and show profound synaptic loss, neurofibrillary tangle formation and gliosis. The amyloid plaques are composed of amyloid β-peptide (Aβ), a 40–42-amino-acid fragment of the β-amyloid precursor protein (APP)[1]. A primary pathogenic role for APP/Aβ is suggested by missense mutations in APP that are tightly linked to autosomal dominant forms of AD[2,3]. A major obstacle to elucidating and treating AD has been the lack of an animal model. Animals transgenic for APP have previously failed to show extensive AD-type neuropathology[4–10], but we now report the production of transgenic mice that express high levels of human mutant APP (with valine at residue 717 substituted by phenylalanine) and which progressively develop many of the pathological hallmarks of AD, including numerous extracellular thioflavin S-positive Aβ deposits, neuritic plaques, synaptic loss, astrocytosis and microgliosis. These mice support a primary role for APP/Aβ in the genesis of AD and could provide a preclinical model for testing therapeutic drugs.

Transgenic mice were generated using a platelet-derived growth factor (PDGF)-β promoter[11] driving a human APP (hAPP) minigene encoding the $APP_{717V\rightarrow F}$ mutation associated with familial AD[12] (PD-APP; Fig. 1*a*). The construct contained APP introns 6–8, allowing alternative splicing of exons 7 and 8.

‡ Present addresses: Department of Biology and Biotechnology, Worcester Polytechnic Institute, 100 Institute Road, Worcester, MA 01609, USA (D.A.); Genzyme Corporation, One Mountain Road, Framingham, MA 01701, USA (P.B.); University of Massachusetts, Department of Veterinarian and Animal Sciences, Amherst, MA 01003, USA (C.B.); Molecular Therapeutics Inc, 400 Morgan Lane, West Haven, CT 06516, USA (T.D.); Transkaryotic Therapies Inc., 195 Albany Street, Cambridge, MA 02139, USA (F.G.); Joint Program in Neonatology, Children's Hospital, Enders, Rm 950, 300 Longwood Avenue, Boston, MA 02115, USA (S.H.); Innovir Laboratories Inc., 510 East 73 Street, New York, NY 10022, USA (P.L.); Alteon Inc., 170 Williams Drive, Ramsey, NJ 07446, USA (M.M.-Z.); Millennium Pharmaceuticals Inc., 640 Memorial Drive, Cambridge, MA 02139, USA (J.V.).
¶ To whom correspondence should be addressed.

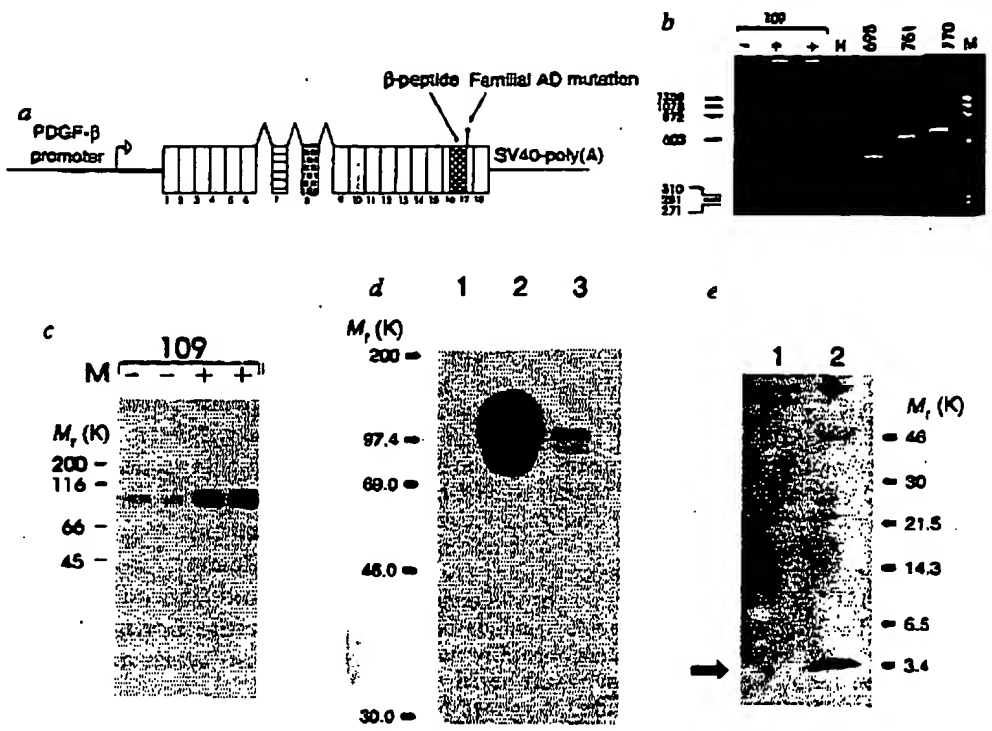

Fig. 1 Analysis of app expression in brain tissue of pd-app transgenic mice. *a*, Map of the APP construct (PD-APP) minigene used to generate transgenic mice (not to scale). The construct contains the PDGF β-chain promoter, full-length hAPP cDNA encoding the Val-to-Phe mutation at codon 717, and the inclusion of genmic sequences for hAPP introns 6–8. *b*, RT-PCR analysis demonstrates the presence of transcripts encoding the 695, 751 and 770 isoforms of hAPP in transgenic animal brains (+) but not in brains from nontransgenic littermates (−). Control reactions using human brain RNA (H) as well as cDNA clones encoding hAPP 695, 751 or 770 are also shown. M, Markers (calibration in bp). *c*, Immunoblot analysis of total APP expression (human and mouse) in transgenic mouse (+) and control littermate (−) brain tissue using a C-terminal APP antibody, α6. *d*, Human-specific APP expression in brain tissue from a 6-month-old nontransgenic littermate (lane 1), transgenic mouse (lane 2) or human AD cortex (lane 3) using immunoblotting with the human-specific APP antibody 8E5. *e*, Immunoprecipitation and immunoblot analysis of Aβ from the brain tissue of a 9-month-old non-transgenic littermate (lane 1) and a 9-month-old transgenic mouse (lane 2).

METHODS. The PDGF β-chain 5′ flanking sequence included 1.3 kb upstream of the transcription initiation site and ~70 bp of 5′ untranslated region, ending at the *Aur*II site[10]. The β-APP sequences were derived from human β-APP cDNA starting with the *Nru*I site in exon 1 through to the end of exon 6 and from the beginning of exon 9 through to exon 18, including the 3′ untranslated sequence ending at the *Sph*I site, and from human genomic sequences from exons 6–9, including all intervening introns. To introduce the familial AD mutation at position 717, Val was mutated to Phe (G to T, using the P-Select mutagenesis kit; Promega). The late SV40 polyadenylation signal was provided by the 240-bp *Bam*HI to *Bcl*I fragment. Plasmid sequences (pUC) were removed by *Sac*1 and *Not*1 digestion before microinjection. Transgenic mice were generated using standard techniques[19], except that PD-APP DNA was microinjected into the embryos at the two-cell stage. Seven founder mice were generated and line 109 was used for extensive analysis. RNA was isolated from brain tissue as described[20] and subjected to RT-PCR as described[21] using human-specific APP primers (5′-CCGATGATGACGAGGACGAT-3′, 5′-TGAACACGTGACGAGGCCGA-3′) with the following PCR conditions: 40 cycles of 1 min at 94 °C, 40 s at 60 °C, 50 s at 72 °C. The identities of the human APP RT-PCR bands from the transgenic mouse RNA were verified by subcloning and sequencing. Analysis of holo-APP involved brain homogenization in 10 volumes of PBS containing 0.5 mM EDTA, 10 μg ml^{-1} leupeptin and 1 mM PMSF. Samples were spun at 12,000*g* for 10 min and the pellets resuspended in RIPA (150 mM NaCl, 50 mM Tris, pH 8.0, 20 mM EDTA, 1.0% deoxycholate, 1.0% Triton X-100, 0.1% SDS, 1 mM PMSF and 10 μg ml^{-1} leupeptin (*d*)). Samples (each containing 30 μg total protein) were analysed by SDS–PAGE, transferred to Immobilon and reacted with either the holo-APP antibody, α6 (ref. 22), or 8E5 monoclonal antibody. 8E5 was prepared against a bacterial fusion protein encompassing hAPP residues 444–592 (ref. 22) and is human-specific showing essentially no crossreactivity against mouse APP (*d*, lane 1). For immunoblot analysis of Aβ (*e*), a 9-month-old mouse brain was homogenized in 5 ml 6 M guanidine HCl, 50 mM Tris, pH 7.5. The homogenate was centrifuged at 100,000*g* for 15 min and the supernatant was dialysed against H_2O overnight adjusted to PBS with 1 mM PMSF and 25 μg ml^{-1} leupeptin. This material was immunoprecipated with antibody 266 resin, and immunoblotted with the human-specific Aβ antibody, 6C6, as described[13].

We used only heterozygous animals. Southern analysis of 104 from four generations showed that ~40 copies of the transgene were inserted at a single site and transmitted in a stable manner (data not shown). Human APP messenger RNA was produced in several tissues of the transgenic mouse, but at especially high levels in brain (not shown). RNase protection assays revealed ~18-fold more APP expression in the brains of line 109 animals than in most previously described lines expressing neuron-specific enolase (NSE)-promoter-driven APP transgenes (not shown; refs 4, 8–10). In addition, the three major splicing variants of hAPP mRNA (695, 751, 770)[1] were expressed in the transgenic mice, as evidenced by reverse-transcriptase polymerase chain reaction (RT-PCR) (Fig. 1*b*). Immunoblot analysis of brain homogenates using either a holo-APP polyclonal antibody or a human-specific APP monoclonal antibody revealed hAPP overexpression in the transgenic mouse at levels ≥10-fold higher than either endogenous mouse APP levels (Fig. 1*c*, *d*) or those in AD brain (Fig. 1*d*). Using human-specific Aβ antibodies, we isolated a 4K Aβ-immunoreactive peptide from the brains of the transgenic animals, which corresponds to the relative molecular mass of Aβ (Fig. 1*e*). Brain levels of Aβ were at least 10-fold higher in line-109 animals than in the previously described hAPP transgenic mice (not shown; ref. 9). Finally, embryonic day-16 cortical cell cultures from transgenic animals constitutively secreted human Aβ, including a substantial fraction of Aβ 1–42 (5 ng ml^{-1} total Aβ; 0.7 ng ml^{-1} Aβ 1–42), as detected in media by human-specific Aβ enzyme-linked immunosorbent assays (not shown; refs 9 and 13). Thus, line-109 animals greatly overexpressed human APP mRNA, holo-APP and Aβ in their brains.

Brains from 18 transgenic animals and 12 age-matched nontransgenic littermate controls (4–13 months old) representing three generations of the line-109 pedigree were extensively examined histopathologically. Between 4–6 months of age ($n=7$), no obvious pathology was detected; however, at ~6–9 months of age ($n=7$), transgenic animals began to exhibit deposits of human Aβ in the hippocampus, corpus callosum and cerebral cortex, but not in other brain regions. These increased with age, and by eight months many deposits (30–200 μm) were seen (Fig. 2*a*). As the animals aged (≥9 months; $n=4$), the density of the plaques increased (Fig. 2*c*) until the Aβ-staining pattern resembled that of AD (Fig. 2*a*, inset). Robust pathology was

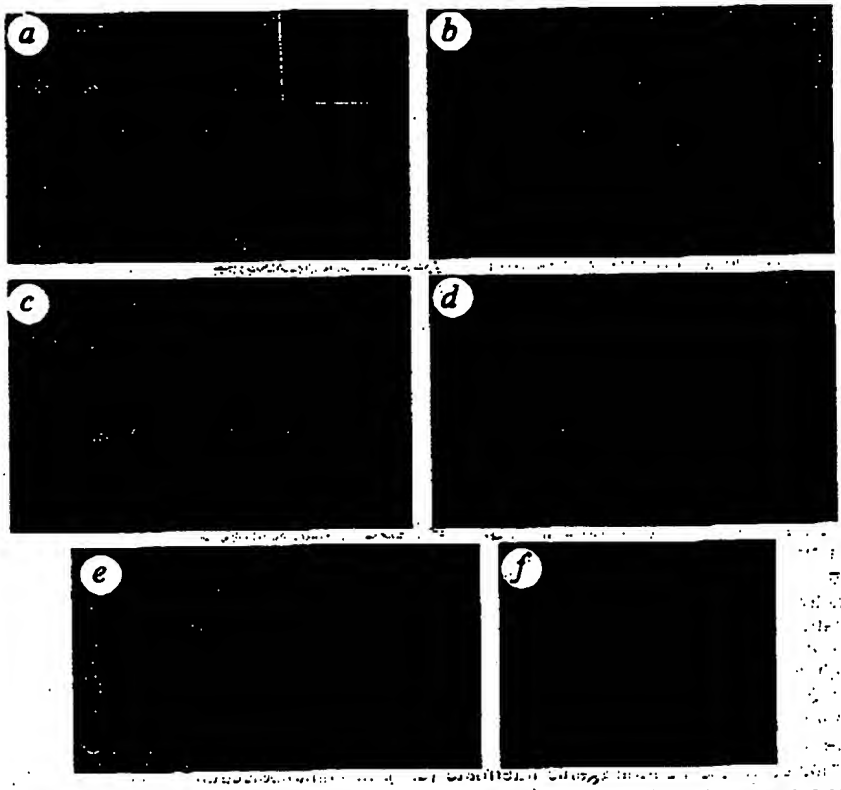

FIG. 2 Demonstration of AD-like amyloid plaques in PD-APP transgenic mice. Human and mouse brain sections were labelled with antiserum R1280 generated against synthetic human Aβ 1–40 peptide. H, Hippocampus; C, cortex; CC, corpus callosum; OML, outer molecular layer of the dentate gyrus; F, hippocampal fissure. Coronal sections of the hippocampus and neocortex from *a*, an 8-month-old transgenic mouse containing Aβ deposits (arrows), and *b*, a non-transgenic littermate. Inset in *a*, human tissue from AD frontal cortex stained with R1280. Adjacent parasagittal sections from a 13-month-old transgenic mouse before (*c*) and after (*d*) preincubation of the antibody with synthetic Aβ 1–40 peptide. In *c*, the large increase in Aβ was confined to the cortex and hippocampus. Several regions of the hippocampus contained densely packed Aβ, including the terminal zone of the perforant pathway in the outer molecular layer of the dentate gyrus (arrowheads). Boxed areas 1 and 2 are shown at higher magnification in *e* and *f*, respectively. Scale bars in *a–d*, 200 μm. In *e*, the outer molecular layer of the dentate gyrus contained areas of compacted and diffuse (asterisk) plaques. The edge of the granule cell layer is visible at the bottom. In *f*, a field of Aβ deposits in the occipital cortex. Scale bars in *e* and *f*, 40 μm.

METHODS. Mouse brains were removed and placed in Trojanowski's fixative[23] for 48 h before paraffin embedding. 6-μm coronal or parasaggital sections from transgenic and non-transgenic mice were placed adjacent to each other on poly-L-lysine coated slides. Sections were deparaffinized, rehydrated, and treated with 0.03% H_2O_2 for 30 min before overnight incubation at 4 °C with a 1:1,000 dilution of the Aβ antibody, R1280 (ref. 24). For absorption studies, synthetic human Aβ 1–40 peptide[25] in 10% aqueous dimethylsulphoxide was added to a final concentration of 7.0 μM to the diluted antibody and incubated for 2 h at 37 °C. The diluent was applied to the sections and processed under the same conditions as the standard antibody solution. Peroxidase rabbit IgG kit (Vector Labs) was then used as recommended, with 3,3'-diaminobenzidine (DAB) as the chromagen. Similarly fixed human AD brain was processed simultaneously under identical conditions.

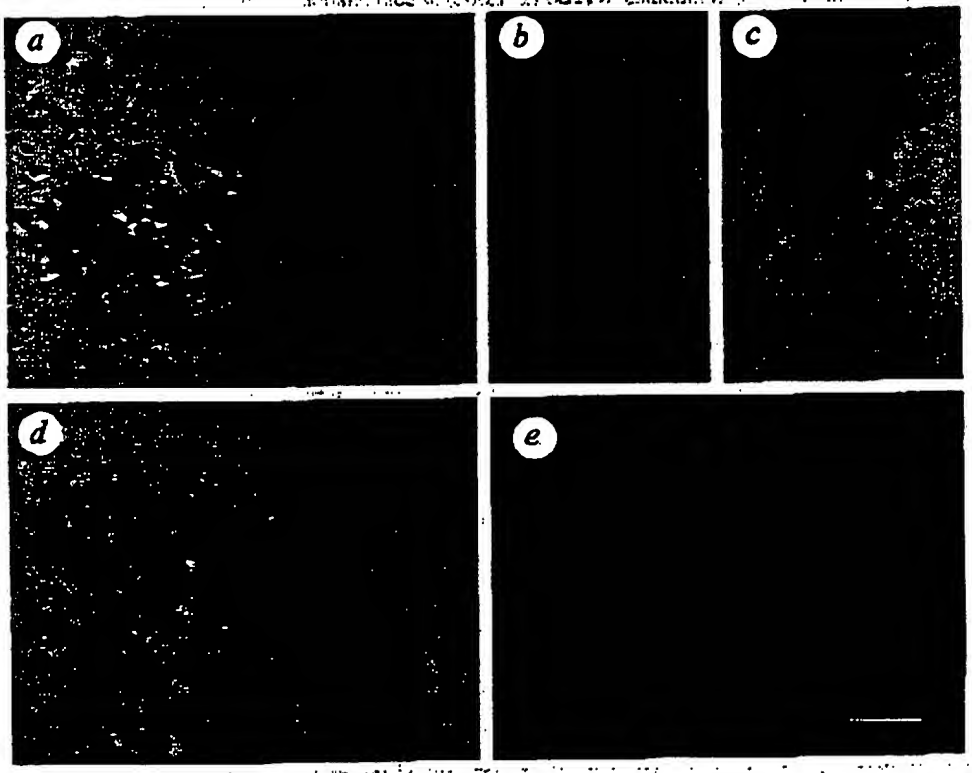

FIG. 3 Morphological diversity of Aβ deposition in the PD-APP mouse brain. Roughly spherical (*a*), and wispy, irregular deposits (*b*), labelled with antibody 9204 (Aβ1–5; ref. 26) specific for the free N terminus of Aβ. *c*, Aβ core and surround labelled with antibody 277-2, specific for the C terminus of Aβ1–42. *d*, Astrocytic gliosis (arrow) associated with Aβ deposition was evident after double immunolabelling with antibodies to glial fibrillary acidic protein (GFAP, red) and human Aβ (Aβ 1–5; brown). *e*, Aβ deposits were also reactive with thioflavin S. A compacted Aβ core and 'halo' is evident in the large plaque. The fine background fluorescence represents autofluorescent lipofuscin granules. Scale bars, 50 μm.

METHODS. For *a–c*, immunochemistry was performed as described for Fig. 2. Antibody 9204 (to Aβ1–5) was used at a concentration of 7.0 μg ml^{-1}. Antibody 277-2, specific for Aβ1–42 (apparent affinity for Aβ1–42 = 75 nM versus >10 μM for Aβ1–40 by radioimmunoassay competition), was prepared by immunizing New Zealand white rabbits with the peptide cysteine-aminoheptanoic acid–Aβ33–42 conjugated to cationized BSA ('Super Carriers'; Pierce) using a typical immunization protocol (500 μg per injection). Specific antibodies were affinity-purified from serum against the immunogen immobilized on agarose beads. Before incubation with 277-2 (10 μg ml^{-1}) sections were treated for 1–2 min with 80% formic acid. In *c*, the antibody 9204 was reacted using the peroxidase rabbit IgG kit (Vect r Labs). The product was then visualized with DAB, and the sections were incubated overnight at 4 °C with a 1:500 dilution of polyclonal anti-GFAP (Sigma). The GFAP antibody was reacted using the alkaline phosphatase anti-rabbit IgG kit and alkaline phosphatase substrate kit I. (Vector Labs; used according to the manufacturer's recommendations). Sections were stained with thioflavin S using standard procedures[27] and viewed with ultraviolet light through an FITC filter of maximum wavelength 440 nm.

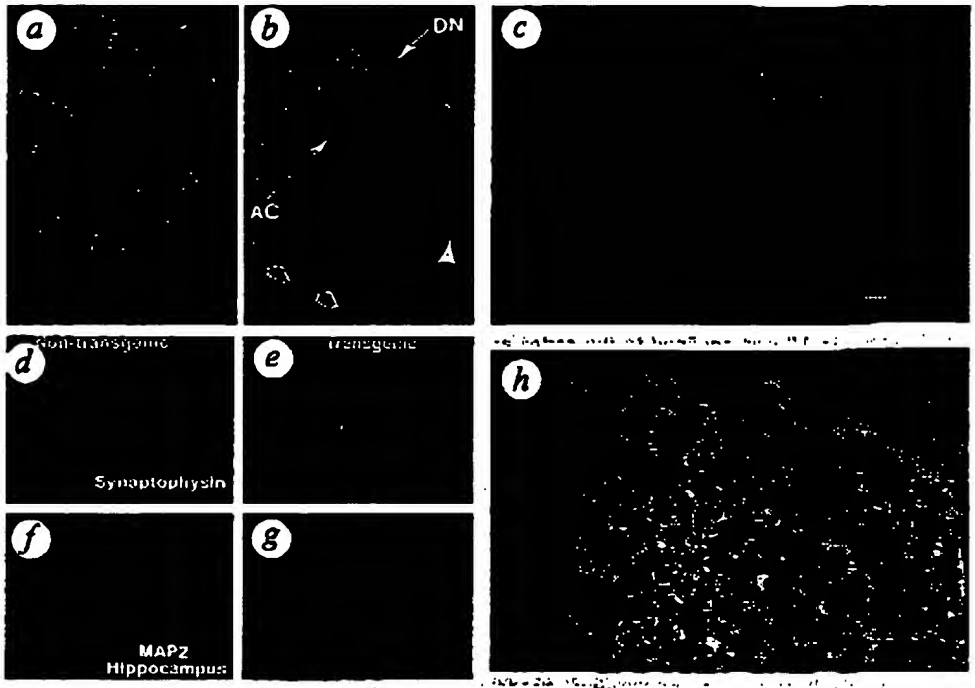

FIG. 4 Laser scanning confocal images of human and 8-month-old transgenic mouse brains, demonstrating th relationship of extracellular cortical Aβ deposit to dystrophic neurites and neuropil abnormalities, as well as the reduction of synaptic density and dendrites in the transgenic hippocampus. An Aβ deposit and adjacent neuropil in an 8-month-old transgenic mouse brain are also shown in an electron micrograph. In both human (*a*) and mouse (*b*) brains, Aβ deposits (red) were associated with distorted neurites (DN) containing synaptophysin (green). Yellow signifies overlap of the two markers. *b*, Aβ immunoreactive plaque in a transgenic mouse brain containing a central amyloid core (AC); synaptic loss (arrowhead) and compression (open arrows) of the neuropil surrounding the amyloid deposit are also evident. *c*, Aβ deposit (red) in a transgenic mouse brain associated with morphologically abnormal hAPP-positive neurites (green). The magnification for *a–g* is indicated by the scale bar in *c* (20 μm). Both synaptophysin (red) and microtubule-associated protein-2 (MAP-2; green) immunostaining were reduced throughout the molecular layer of the hippocampal dentate gyrus in the transgenic mouse (*e*, *g*) compared to the non-transgenic littermate (*d*, *f*). *h*, Immunoelectron micrograph of a transgenic mouse brain demonstrating extracellular Aβ deposition (A) decorated with the human-specific R1280 Aβ antiserum (outlined by arrows). A dystrophic neurite (DN) in the immediate vicinity of the Aβ deposit contained abundant large mitochondria (M) and lamellar dense bodies (LB). Scale bar, 2 μm.

METHODS. 40-μm-thick vibratome sections were incubated overnight at 4 °C with the following antibodies: R1280 (1:1,000) in combination with polyclonal anti-synaptophysin in *a* and *b* (1:150; Dako) or 8E5 in *c* (7.0 μg ml^{-1}; described in Fig. 1). For *d–g*, sections were incubated with anti-synaptophysin or monoclonal anti-MAP 2 (1:20, Boehringer-Mannheim), and reacted with a goat anti-rabbit biotinylated antibody (1:100) followed by a mixture of FITC-conjugated horse anti-mouse IgG (1:75) and avidin D Texas red (1:100) (Vector Labs). The double-immunolabelled sections were viewed on a Zeiss Axiovert 35 microscope with attached laser confocal scanning system MRC 600 (Bio-Rad). The Texas red channel collected images of the R1280 (*a*, *b*, *c*) or synaptophysin (*d*, *e*) labelling, and the FITC channel collected synaptophysin (*a*, *b*), 8E5 (*c*), or MAP 2 (*f*, *g*) labelling. Optical *z*-sections 0.5 μm in thickness were collected from each region; details of similar image processing and storage are described in ref. 28. For immunoelectron microscopy, mice were perfused with saline followed by 2.0% paraformaldehyde and 1.0% glutaraldehyde in cacodylate buffer. 40-μm-thick vibratome sections were incubated with R1280, and reacted as in Fig 2. Immunolabelled sections with Aβ deposits were then fixed in 1.0% ammonium tetraoxide and embedded in epon/araldite before viewing ultrathin sections with a Jeol CX100 electron microscope[29].

also seen in another transgenic line generated from the PD-APP vector (line 35; data not shown). Aβ deposits of varying morphology clearly were evident as a result of using a variety of Aβ antibodies, including well characterized human-specific Aβ antibodies (Figs 2, 3) and antibodies specific for the free amino and carboxy termini of Aβ 1–42 (Fig. 3*a–c*). Serial sections demonstrated many plaques were positively stained with both of the latter antibodies. The forms of the Aβ deposition ranged from diffuse irregular types to compacted plaques with cores (Fig. 3). Non-transgenic littermates (Fig. 2*b*) showed none of these neuropathological changes. Immunostaining was fully absorbable with the relevant synthetic peptide (Fig. 2*d*), and was apparent using a variety of processing conditions, including fixation with paraformaldehyde and Trojanowski methods (Figs 2, 3). Many plaques were stained with thioflavin S (Fig. 3*e*), and some were also stained using the Bielschowsky silver method and were birefringent with Congo red (not shown), indicating the true amyloid nature of these deposits. Confirmation of the presence f extracellular Aβ was obtained using immunoelectr n microscopy (Fig. 4*h*). The majority of plaques were intimately surrounded by GFAP-positive reactive astrocytes (Fig. 3*d*), similar to the gliosis found in AD plaques. The neocortices of the transgenic mice contained diffusely activated microglial cells, as defined by their am eboid appearance and shortened processes (not shown). Preliminary attempts t identify neurofibrillary tangles with tau antibodies were negative, consistent with their well known absence in rodent tissues[14]. Nevertheless, clear evidence for neuritic pathology was apparent using both conventional and confocal immunomicroscopy. Many Aβ plaques were closely associated with distorted neurites that could be detected with hAPP-specific antibodies (Fig. 4*c*) and with anti-synaptophysin antibodies (Fig. 4*b*), suggesting that these neurites were derived in part from axonal sprouts, as observed in the AD brain (Fig 4*a*). The plaques compressed and distorted the surrounding neuropil (Fig. 4*b*), also as in the AD brain (Fig. 4*a*). Finally, synaptic and dendritic density were reduced in the molecular layer of the hippocampal dentate gyrus of the transgenic mice. This was evident by reduced immunostaining for the presynaptic marker synaptophysin (compare Fig. 4*d* and *e*) and the dendritic marker MAP-2 (compare Fig. 4*f* and *g*), as described in AD brain[15].

Several transgenic rodent lines have been produced that express either the hAPP gene or hAPP complementary DNAs regulated by a variety of promoters[4–10]. In particular, NSE-driven APP_{751} transgenic mice[9,10] have sparse Aβ deposits which are more typical f early AD and young D wn's syndrome cases; in these mice, unlike ours, mature lesi ns such as frequent compacted plaques, neuritic dystr phy and extensive gliosis were very rare[10]. Our success in generating AD-like pathology consistently in these transgenic mice is probably due to the construct used and the high level of hAPP expression. The transgen contains a splicing cassette that permits expression of all three major hAPP isof rms. Expression is driven by the PDGF-β promoter, which is known to target expression preferentially to neurons

of the cortex, hippocampus, hypothalamus and cerebellum of transgenic animals[11]. The familial AD mutation at residue 717[12] may be important as it partially shifts production of Aβ from the 40-amin -acid form to the m re amyloidogenic 42-residue peptide known to predominate in plaques[16,17]. Preparation of APP transgenic mice independently harbouring each f these features will be required t identify the essential component(s) that result in pathology.

The most notable feature of these transgenic mice is their Alzheimer-like neuropathology, which includes extracellular Aβ deposition, dystrophic neuritic components, gliosis and loss of synaptic density with regional specificity resembling that of AD. Based on the limited sampling to date, plaque density appears to increase with age in these transgenic mice, as it does in humans[1], implying a progressive Aβ deposition that exceeds its clearance, as also proposed for AD[18]. Our transgenic model provides strong new evidence for the primacy of APP expression and Aβ deposition in AD neuropathology and offers a means to test whether compounds that lower Aβ production and/or reduce its neurotoxicity *in vitro* can produce beneficial effects in an animal model prior to advancing such drugs into human trials. □

Received 17 October 1994; accepted 5 January 1995.

1. Selkoe, D. J. A. *Rev. Neurosci.* **17**, 489–517 (1994).
2. Haroy, J. *Clin. geriatr. Med.* **10**, 239–247 (1994).
3. Mann, D. M. A. *et al. Neurodegeneration* **1**, 201–215 (1992).
4. Quon, D. *et al. Nature* **352**, 239–241 (1991).
5. Sanhu, F. A., Salim, M. & Zain, S. B. *J. biol. Chem.* **266**, 21331–21334 (1991).
6. Lamb, B. T. *et al. Nature Genet.* **5**, 22–30 (1993).
7. Pearson, B. E. & Choi, T. K. *Proc. natn. acad. Sci. U.S.A.* **90**, 10578–10582 (1993).
8. Mucke, L. *et al. Brain Res.* **688**, 151–167 (1994).
9. McConlogue, L. *et al. Neurobiol. Aging* **15**, S12 (1994).
10. Higgins, L. S. *et al. Ann. Neurol.* **35**, 598–607 (1994).
11. Sasshara, M. *et al. Cell* **64**, 217–227 (1991).
12. Murrell, J. *et al. Science* **254**, 97–99 (1991).
13. Seubert, P. *et al. Nature* **359**, 325–327 (1992).
14. Cork, L. C. *et al. J. Neuropath. exp. Neurol.* **47**, 629–641 (1988).
15. Masliah, E. *et al. Am. J. Path.* **138**, 235–246 (1991).
16. Suzuki, N. *et al. Science* **264**, 1336–1340 (1994).
17. Roher, A. *et al. J. biol. Chem.* **268**, 3072–3083 (1993).
18. Maggio, J. E. *et al. Proc. natn Acad. Sci. U.S.A.* **89**, 5462–5466 (1992).
19. Hogan, B., Constantini, F. & Lacey, E. in *Manipulating the Mouse Embryo: A Laboratory Manual* (Cold Spring Harbor Laboratory, Cold Spring Harbor, NY, 1986).
20. Chomczynski, P. & Sacchi, N. *Analyt. Biochem.* **162**, 156–159 (1987).
21. Wang, A. M. *et al. Proc. natn. Acad. Sci. U.S.A.* **86**, 9717–9721 (1989).
22. Ottersdorf, T. *et al. J. biol. Chem.* **265**, 4492–4497 (1990).
23. Arai, H. *et al. Proc. natn. Acad. Sci. U.S.A.* **87**, 2249–2253 (1990).
24. Tamaoka, A. *et al. Proc. natn. Acad. Sci. U.S.A.* **89**, 1345–1349 (1992).
25. Games, D. *et al. Neurobiol. Aging* **13**, 569–576 (1992).
26. Saido, T. C. *et al. J. biol. Chem.* **269**, 15253–15257 (1994).
27. Dickson, D. W. *et al. Acta neuropath.* **79**, 486–493 (1990).
28. Masliah, E. *et al. J. Neuropath. exp. Neurol.* **52**, 619–632 (1993).
29. Masliah, E. *et al. Acta neuropath.* **81**, 428–433 (1991).

ACKNOWLEDGEMENTS. We thank M. Mallory, A. Maya, N. Ge, E. Rockenstein, O. Stephenson and E. Johnstone for technical assistance; the animal care technicians involved in this project; J. Trojanowski for human brain sections; T. Saido and D. Selkoe for anti-Aβ antibodies 9204 and R1280, respectively; T. Collins and D. Goldgaber for the PDGF promoter and APP cDNA subclones, respectively; and D. Selkoe for helpful comments and advice.

Gating of the voltage-d pendent chloride channel ClC-0 by the permeant anion

Michael Pusch, Uwe Ludewig, Annett Rehfeldt* & Thomas J. Jentsch†

Centre for Molecular Neurobiology (ZMNH), Hamburg University, Martinistrasse 52, D-20246 Hamburg, Germany

CHLORIDE channels of the ClC family are important for the control of membrane excitability[1–3], cell volume regulation[4,5], and possibly transepithelial transport[6,7]. Although lacking the typical voltage-sensor found in cation channels[8–10], gating of ClC channels is clearly voltage-dependent. For the prototype *Torpedo* channel ClC-0 (refs 11–15) we now show that channel opening is strongly facilitated by external chloride. Other less permeable anions can substitute for chloride with less efficiency. ClC-0 conductance shows an anomalous mole fraction behaviour with Cl^-/NO_3^- mixtures, suggesting a multi-ion pore. Gating shows a similar anomalous behaviour, tightly linking permeation to gating. Eliminating a positive charge at the cytoplasmic end of domain D12 changes kinetics, concentration dependence and halide selectivity of gating, and alters pore properties such as ion selectivity, single-channel conductance and rectification. Taken together, our results strongly suggest that in these channels voltage-dependent gating is conferred by the permeating ion itself, acting as the gating charge.

The *Torpedo* electric organ Cl^--channel ClC-0 (ref. 12) has a 'slow' gate operating on both pr tochannels of the double-barrelled channel[13,14] simultaneously, and a 'fast' gate acting on single protochannels[13–15]. Both gates have opposite voltage-dependence, with the fast gate being opened by depol rization.

ClC-0 was expressed in *Xenopus* oocytes and the fast gate was studied in isolation (Fig. 1*a*). The dependence of the steady-state open probability, p_{open}, on the transmembrane voltage V can be described by the Boltzmann distribution $p_{open} = 1/(1+\exp(z_n e_0(V_{1/2}-V)/kT))$ (where e_0 is the elementary charge, $V_{1/2}$ is the voltage of half-maximal activation, k is the Boltzmann constant, and T is the temperature) with a nominal gating charge $z_n \sim 1$ in agreement with earlier data[13,14]. Consistent with single-channel measurements[13,14], gating kinetics indicate a two-state gating mechanism. Reducing extracellular Cl^- concentration ($[Cl^-]_o$) shifts $p_{open}(V)$ to positive voltages without significantly changing its slope (the gating charge) (Fig. 1*b*). In contrast, intracellular chloride has little effect (Fig. 1*c*). A dependence of ClC-0 microscopic gating transitions on the Cl^--gradient has already been noted[15].

The dependence of gating on $[Cl^-]_o$ could be due to a simple mechanism in which channel opening depends on chloride binding to a site within the pore; p_{open} should then increase with $[Cl^-]_o$ and with positive intracellular potentials. Intracellular chloride has little effect on gating, because it cannot reach its binding site in the closed state.

The simplest model assumes that chloride-binding to a single site in the pore is required for channel opening[10]. Although it may serve as a first approximation to our data, the shift of p_{open} with $[Cl^-]_o$ is ~20% less than minimally predicted[10]. This suggests that this model is either principally unsuited to explain ClC-0 gating, or that it needs further refinement.

The pores of many channels, including certain chloride channels[16], can accommodate more than one ion, leading to concentrati n-dependent interactions within the pore. In a single-ion pore, conductance changes monot nously when the concentration ratio between two permeant ionic species is varied; in a multi-ion pore, however, interactions between different species can lead to a current minimum at a certain concentration ratio, an 'anomalous mole fraction behaviour'[16,17]. We indeed found this effect with mixtures of Cl^- and NO_3^- (Fig. 2*b*), indicating that ClC-0 has a multi-ion pore. Thus, a mod l having a singl chloride-binding site[10] may be too simplistic.

* Deceased.
† To whom correspondence should be addressed.